Rain initiation time in turbulent warm clouds

student Marija Vucelja, adviser Prof. Dr. Gregory Falkovich

M.Sc. Thesis

5th December 2005

We study rain initiation time in warm clouds; clouds where droplets grow by vapor condensation and coalescence due to collisions. These growth mechanisms are accompanied by raindrop loss due to fallout. We present a mean-field model of droplet growth in warm clouds. The model allows for an effective numerical simulation. We apply the numerical scheme that is conservative in water mass and keeps accurate count of the number of droplets, to study how the rain initiation time depends on different parameters. In particular, we show that the rain initiation time depends non-monotonically, actually it has a minimum, on the number of cloud condensation nuclei. We also present a simple model that allows one to estimate the rain initiation time for turbulent clouds with an inhomogeneous concentration of cloud condensation nuclei. We argue that over-seeding even a part of a cloud by small hygroscopic nuclei one can substantially delay the onset of precipitation. This work was done together with Dr. Michael G. Stepanov and is accepted by the Journal of Applied Meteorology.

Contents

1. Introduction

Strepsiades: Tell me, do you think Zeus always rains
new water down
Or does the sun draw the old up to be re-used?
Amynias: I don't know and I don't care.
Strepsiades: How do you expect to get your money if you
know nothing
Of meteorology?

Aristophanes, CLOUDS, trans.
Moses Hadas, New York
Bantam Books, 1962, p. 136.

Water vapor evaporates from the land or sea, and the moist air, warmed by heat from the ground, rises up and cools. Eventually, the vapor condenses on aerosols into micron-size droplets. These droplets collect more vapor until they reach diameters of about 10 to 20 micrometers. Then they are heavy enough to be significantly influenced by gravity, and their growth continues by coalescence due to collisions. Finally they form raindrops (millimeter-size drops), that are pulled back to earth by gravity. Droplets of fine drizzle are 200 micrometers or so in diameter, and fall at about half a meter per second. Those with diameters of about a millimeter plunge earthwards at about nine meters per second. This is how rainfall occurs in *warm clouds*[1] (Pruppacher and Klett, 1997; Seinfeld and Pandis, 1998).

1 *Warm clouds* are clouds without ice particles in them. Temperatures in such clouds reach sometimes even below $-10°C$, therefore a part of the meteorological community considers this designation somewhat inappropriate (Pruppacher and Klett, 1997).

Processes of vapor condensation on *cloud condensation nuclei*[2] (CCN) and droplet growth by coalescence due to collisions can be modelled by the equation for the local distribution of droplets over sizes, $n(\mathbf{r}, t, a)$ (cm^{-4}) and the water vapor density, $M(\mathbf{r}, t)$ ($\mathrm{g} \cdot \mathrm{cm}^{-3}$). These variables depend on *supersaturation*[3] s, air velocity $\mathbf{u}(\mathbf{r}, t)$ and velocities of cloud particles $\mathbf{v}(\mathbf{r}, t, a)$. Thus to equations describing evolutions of the water vapor content and the local distribution of droplets over sizes one must also add the equation that describes the temperature changes (determines s) and Navier-Stokes equations for the velocities. Such a system cannot be possibly solved numerically with any meaningful resolution, neither presently, nor in a foreseeable future. One of the obstacles to a deeper understanding of rainfall phenomena is it's multi-scale nature. Relevant scales enclose those of warm and cold *fronts*[4] stretching over hundreds of kilometers, of individual clouds - a few kilometers across, of tiny eddies - perhaps a few centimeters across and the viscous scale of the order of millimeters. The spatial structure of the fields involved is very complicated, particularly due to cloud turbulence. Reynold's number in clouds ranges between $10^6 - 10^9$.

Our aim in this thesis is to formulate some mean-field model which does not contain spatial arguments at all. The requirements to this model are that it must give the correct qualitative relations between the parameters and reasonable quantitative description (at least within the order of magnitude) of the real-world timescales.

We use the model to study the evolution of the local distribution of droplets over sizes, $n(a, t)$ starting from micron sizes all the way to the moment when droplet fallout significantly decreases the water content in the cloud. We call this moment the *rain initiation time* and study how that time depends on initial vapor content and CCN concentration. Our model demonstrates non-monotonic dependence of the rain initiation time on CCN concentration.

We also give an application of this model to an inhomogeneous case (described in Chapter 5), where we show that one can increase the rain initiation time even for a cloud only partially seeded by hygroscopic aerosols. We estimate such seeding is practical. Postponing precipitation of Mediterranean maritime clouds is very valuable to Israel, since then

2 *Cloud condensation nuclei* are hygroscopic aerosol particles, *i.e.* aerosol particles that have a tendency to absorb moisture from humid air. They can serve as nuclei of atmospheric cloud droplets (AMS Glossary, 2000).

3 *Supersaturation* is the condition existing in a given portion of the atmosphere (or other space) when the relative humidity is greater than 100%, that is, when it contains more water vapor than is needed to produce saturation with respect to a plane surface of pure water or pure ice (AMS Glossary, 2000). Here we define supersaturation as $s = 1 - M_{sat}/M$, where M_{sat} is the saturated water vapor density.

4 *Front* in meteorology is the interface or transition zone between two air masses of different density (AMS Glossary, 2000).

these clouds would rain over mainland, instead of raining over the sea!

Beyond the scope of our model are effects related to spatial inhomogeneities and fluctuations of the fields. According to the two basic phenomena involved (condensation and collisions), the main effects are:

- mixing and diffusion of water vapor, heat and droplets, and
- the influence of cloud turbulence on collisions.

We briefly address the first phenomenon in Chapter 5 considering inhomogeneously seeded clouds. We do not consider here the controversial subject of collision enhancement by turbulence giving in Chapter 4 references to the relevant literature.

The structure of the text is the following: in Chapter 2 we introduce the "full cloud model" and give orders of magnitude of changes of relevant variables, also we introduce our mean-field model. Following in Chapter 3 we consider the mean-field model including only collisions in droplet growth, while in Chapter 4 we consider *ab initio* the growth of droplets in clouds including both condensation and collisions mechanisms. Chapter 5 is a study of inhomogeneously seeded clouds with estimates on it's practical aspects.

2. Growth model of droplets in warm clouds

2.1 A realistic cloud

Description of growth of droplets up to precipitation stages in clouds is not a task of cloud microphysics alone. The essence of the complexity of cloud modelling was well expressed by B. J. Mason in his book *The Physics of Clouds* [1] about fifty years ago. Mason emphasizes that for a full description of clouds it is important to recognize that the micro-physical processes (nucleation processes, vapor diffusion, collection, breakup and fallout of droplets, ice enhancement and melting [2]) are largely controlled by the atmospheric motions, which Mason calls *cloud dynamics*. More specifically *cloud dynamics* is the application of fluid dynamics principles to the air motions in clouds and their immediate environments. Hence a quite realistic description[3] of cloud formation and rain initiation time, can be represented with the following set of equations

$$\frac{\partial M}{\partial t} + (\mathbf{u}\cdot\nabla)M - \kappa\nabla^2 M = -4\pi\kappa s M \int an(a)da, \tag{2.1}$$

$$\frac{\partial \mathbf{u}}{\partial t} + (\mathbf{u}\cdot\nabla)\mathbf{u} - \nu\nabla^2\mathbf{u} = -\nabla p + \mathbf{f} + \beta\mathbf{g}T, \tag{2.2}$$

$$\frac{\partial T}{\partial t} + (\mathbf{u}\cdot\nabla)T - \kappa_T\nabla^2 T = -\frac{L_e}{c}\left[\frac{\partial M}{\partial t} + (\mathbf{u}\cdot\nabla)M\right], \tag{2.3}$$

$$\frac{\partial n(a)}{\partial t} + (\mathbf{v}\cdot\nabla)n(a) = -\frac{ks}{\rho_0}\frac{\partial}{\partial a}\frac{n(a)}{a} + \int da'\left[\frac{K(a',a'')n(a')n(a'')}{2(a''/a)^2} - K(a',a)n(a')n(a)\right], \tag{2.4}$$

$$\frac{\partial \mathbf{v}}{\partial t} + (\mathbf{v}\cdot\nabla)\mathbf{v} = (\mathbf{u}-\mathbf{v})/\tau + \mathbf{g}\,. \tag{2.5}$$

Water vapor density $M(\mathbf{r},t)$ changes (2.1) by air induced diffusion and convection, and condensation on surfaces of CCN and water droplets (see Section 2.2 for details). Air velocity

1 See preface to the first edition, B. J. Mason, *The Physics of Clouds* (Clarendon Press, Oxford 1971).
2 The later two are not relevant for warm clouds.
3 Here electrical and chemical effects are neglected.

$\mathbf{u}(\mathbf{r},t)$ is described by the Navier-Stokes equation (2.2) including atmospheric pressure p, buoyancy forces $\beta\mathbf{g}T$ (β is the coefficient linking density changes with temperature changes) and $\mathbf{f}$ forces that can not be expressed like pressure changes or buoyancy forces (usually originating from cloud boundary conditions). Temperature $T(\mathbf{r},t)$ is modelled with the advection-diffusion equation (2.3); it is convected and diffused by air (κ_T is the thermal diffusivity) and decreased due to condensation (L_e is the latent heat of evaporation of water per unit mass, c is the heat capacity of humid air at constant pressure). The evolution of the local droplet distribution over sizes $n(\mathbf{r},t,a)$ is given by (2.4) and explained below in Section 2.2. The last of this set of equations (2.5) describes the evolution of the velocity of a cloud particle $\mathbf{v}(\mathbf{r},t,a)$ through air under the influence of gravity. Note that in clouds it can be typically assumed $\nabla\cdot\mathbf{u}(\mathbf{r},t)=0$ and $\nabla\cdot\mathbf{v}(\mathbf{r},t,a)=0$, since both velocities are much smaller than the corresponding sound velocity. Notations of used variables are represented in Table A.1.

Clouds among themselves differ in shape, size and characteristic values of $M(\mathbf{r},t)$, $\mathbf{u}(\mathbf{r},t)$, $T(\mathbf{r},t)$, $n(\mathbf{r},a,t)$ and $\mathbf{v}(\mathbf{r},a,t)$. Warm precipitating clouds have water vapor densities are between $1-10^{-2}$ g$\cdot$cm^{-3}. Cloud particles range from characteristic sizes of condensation nuclei ($\geq 10^{-2}$ μm) to precipitation particles (≤ 1 mm for raindrops). Concentrations of cloud particles in warm precipitating clouds are between 10^6-10^8 cm^{-3}. The range of relevant cloud-air motion varies from the characteristic size of turbulent eddies which are small enough to decay directly through viscous dissipation ($\geq 10^{-2}$ cm), since it is these eddies that define the characteristic shearing rates for turbulent aerosol coagulation processes, to motion of scales large at least as the cloud itself (>1 km). Reynold's number of clouds range between 10^6-10^9. Thus there are seven orders of magnitude in scales of eddy sizes, two orders of magnitude in concentration of cloud particles, six orders of magnitude in cloud particle sizes, two order of magnitude in water vapor change and one order of magnitude in temperature change and etc. Hence nine interacting and strongly fluctuating fields ($M(\mathbf{r},t)$, $\mathbf{u}(\mathbf{r},t)$, $T(\mathbf{r},t)$, $n(\mathbf{r},t,a)$ and $\mathbf{v}(\mathbf{r},t,a)$) define this realistic cloud model, that awaits a new generation of computers.

2.2 Introduction of the mean-field model

In warm clouds, droplets grow by vapor condensation on cloud condensation nuclei (CCN) and by coalescence due to collisions until as raindrops they fall out of the cloud, see *e.g.* Pruppacher and Klett (1997). Those processes we modelled by the equation for the local distribution of droplets over sizes, $n(\mathbf{r},t,a)\equiv n(a)$ (2.4) and the water vapor density,

$M(\mathbf{r},t)$ ($\mathrm{g\cdot cm^{-3}}$) (2.1). The first term in the right-hand side of (2.4) is due to condensation which changes the droplet size a according to $da^2/dt = 2ks$ where s is supersaturation and the effective diffusion rate k (depending on M) is given by (13.28) from Pruppacher and Klett (1997): $k^{-1} = \kappa^{-1}(\rho_0/M) + \kappa_T^{-1}(\mathcal{L}\mathcal{M}_\mathcal{W}/RT)^2$. Here κ is vapor diffusivity and κ_T is thermal conductivity, $\mathcal{L}$ is the latent heat of condensation, $\mathcal{M}_\mathcal{W}$ is the molecular weight of water, R is molar gas constant, $\rho_0 = 1\,\mathrm{g\cdot cm^{-3}}$ is the density of liquid water. This equation for the condensational droplet growth neglects curvature and solute effects which is valid for sufficiently large droplets (over one micron). The second term in the rhs of (2.4) describes coalescence due to collisions, here $a'' = (a^3 - a'^3)^{1/3}$ is the size of the droplet that produces the droplet of size a upon coalescence with the droplet of size a'. The collision kernel is the product of the target area and the relative velocity of droplets upon the contact: $K(a,a') \simeq \pi(a+a')^2\Delta v$. According to the recent precise measurements (Beard et al, 2002) the *coalescence efficiency*[4] for minimally charged cloud drops of 55-105 μm radius, in a radius ratio range of 0.5 to 1.0, freely falling in air, is likely to be greater than 95%. Since this is the relevant interval of droplet sizes of our problem, we put coalescence efficiency to be unity in our calculations.

At present the description of the full system of equations, shown at the beginning of this chapter, is impossible to model numerically, therefore we spatially averaged equations (2.1) and (2.4) and in this way obtained from them a closed pair. Supersaturation was taken as a constant parameter[5]. The analytic averaging was done by Falkovich et al (1999), by introducing a correction factor to the collision kernel $K(a_1,a_2) \to \langle K(a_1,a_2)n(a_1)n(a_2)\rangle / \langle n(a_1)\rangle\langle n(a_2)\rangle$. However this correction is negligible for gravity dominated collisions and was not used here. Basically we replaced the mean of a product with a product of means[6].

4 *Coalescence efficiency* - the fraction of all collisions between water drops of a specified size that results in actual merging of the two drops into a single larger drop (AMS Glossary, 2000).

5 Supersaturation changes with temperature and temperature changes are slow (see Section 2.1).

6 There also is another problem of neglecting correlations in (2.4). The two-particle probabilities $n_2(a_1,a_2)$ are replaced via the multiplication of one-particle probabilities $n(a_1)n(a_2)$. The assumption is that there is no prehistory of colliding droplets. It is a very good assumption since usually droplets are "born" at distant, "independent" places and do not influence each other prior to their collision (Pruppacher and Klet, 1997).

3. Growth by gravitational collisions

Collisions are negligible for micron-size droplets (Pruppacher and Klett, 1997) for the parameters typical for warm precipitating clouds ($sM/\rho_0 = 10^{-8}$ through 10^{-9} and $10^6 < n = \int n(a)\,da < 10^9\,\mathrm{m}^{-3}$). Droplets larger than couple of microns, have negligible Brownian motion and the collision kernel in still air is dominantly due to gravitational settling:

$$K_g(a,a') = \pi(a+a')^2 E(a,a')|u_g(a) - u_g(a')|\ , \tag{3.1}$$

where u_g is the fall velocity of droplets and E is the collision efficiency - the fraction of all water drops in the path of a falling larger drop that make contact with the larger drop (AMS Glossary, 2000).

3.1 The fall velocity

Once formed, cloud particles immediately begin to move under the action of gravity and frictional forces, the latter arising from their motion through air. The fall velocity u_g is determined by the balance of gravity force $4\pi g\rho_0 a^3/3$ and the drag $F(u_g, a)$. The drag force depends on the Reynolds number of the flow around the droplet, $Re_a \equiv u_g a/\nu$. When Re_a is of order unity or less, $F = 6\pi\nu\rho a u_g$ and $u_g = g\tau$ where ρ is the air density and $\tau = (2/9)(\rho_0/\rho)(a^2/\nu)$ is the so called Stokes time. We use $u_g = g\tau$ for $a < 40$ μm and take $u_g(a)$ from the measurements of Gunn and Kinzer (1949) for $a > 50$ μm with a smooth interpolation for 40 μm $< a <$ 50 μm, as shown in Figure 3.1. The dotted straight lines have slopes 2, 1 and 1/2. One can see that $u_g \propto a^2$ at $a < 40$ μm. There is an intermediate interval with an approximately linear law $u_g \propto a$ for 40 μm $< a <$ 400 μm. When $Re_a \gg 1$ one may expect $F \propto \rho a^2 u_g^2$ as long as droplet remains spherical; that gives $u_g \propto \sqrt{ag\rho_0/\rho}$. Square-root law can be distinguished between 400 μm and 1 mm, while the growth of $u_g(a)$ saturates at larger a due to shape distortions. Gunn and Kinzer's measurement even though done fifty years ago, is still one of the most accurate and representative ones (Pruppacher and Klet, 1997). They measured distilled water droplets

in stagnant air at 760 mm pressure (sea level), temperature 20°C and relative humidity 50%, with accuracy better than 0.7%. Fall velocities for larger drops depend significantly on pressure, therefore at cloud heights fall velocities of those drops differ from Gunn's and Kinzer's values. However drops we consider are small enough so that their measurements, even though done at 760 mm pressure, are good enough.

Also interesting to note is that the drag on rigid spheres and on water drops falling in air coincides well for drop radii below 500 μm (Pruppacher and Klet, 1997). At larger sizes, the drag on drops progressively increases above that for rigid spheres. In order to explain this behavior one must consider their internal circulation, their distortion from a spherical shape and their oscillations, however these drops are already beyond our domain of relevant sizes.

3.2 Collision efficiency

Although in principle the collision problem is a many-body problem, droplet concentrations in natural clouds are low enough that only the interaction of pairs of droplets need to be considered. It is experimentally verified that the shape-distortions which may occur when the drops are in close proximity may thus be considered of secondary importance in most cases of interest.

The essential piece of information to be extracted from a study of the collision model described above is the effective cross-section for the collisions of the two spheres - the *collision efficiency*. Assuming the initial vertical separation for unequal droplets is large enough, so that they fall independently in the beginning, the only parameters which could play a role in the interaction process are a_1, a_2, the kinematics viscosity, the air and water density, the gravity acceleration and the horizontal offset of droplets; thus $E = E(a_2/a_1, a_1, R_{e_a})$. For equal droplets, this condition must be altered slightly - there one starts with a vertical separation such that hydrodynamical interaction between droplets is at a threshold.

As a consequence of the tendency for deflection by viscous forces from the collision trajectory, one can anticipate that generally $E < 1$ (expect for $a_2/a_1 \to 1$, see below). Since the forces of deflection must become less effective as the inertia of spheres increases, E should be a monotonic increasing function of a_1. For the same reason, E also should be a monotonic increasing function of a_2/a_1, at least for $a_2/a_1 \ll 1$. The situation for a_2/a_1 approaching unity is not obvious, there the relative approach velocity decreases so that small forces of deflection have a relatively long time to operate and hence to prevent

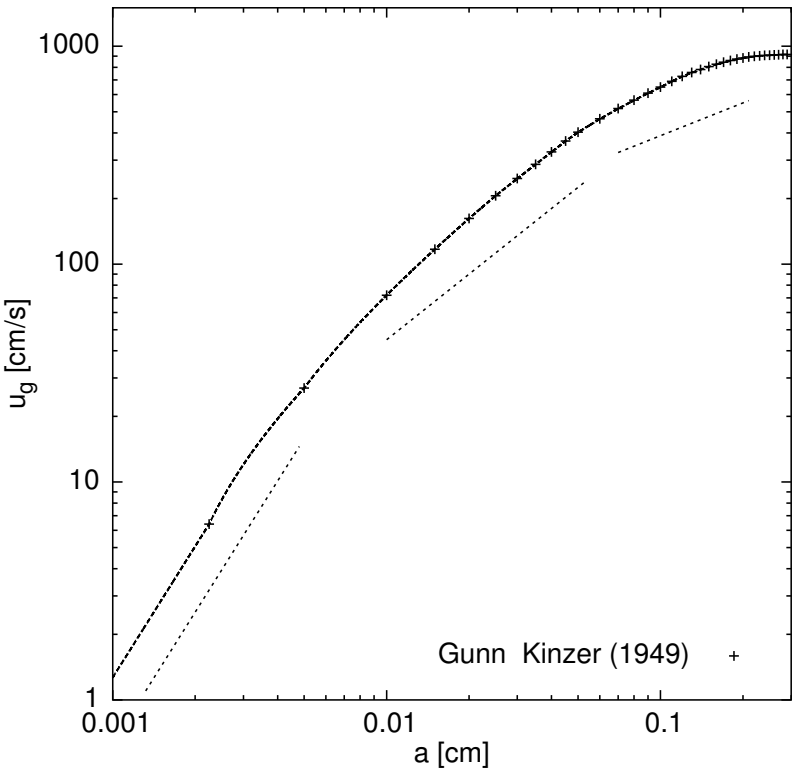

Figure 3.1: *Terminal fall velocity u_g as a function of cloud droplet radius a, obtained by interpolating Gunn's and Kinzer's measurements and extrapolating the laminar part by Stokes flow formula. Measurements were done in* 1949, *at* 760 mm *pressure, temperature* 20°C *and relative humidity* 50%, *with accuracy better than* 0.7%.

a collision, on the other hand, there is a possibility of *wake capture* as the trailing sphere falls into the wake of a leading sphere, and thus encounters less resistance to motion than the latter.

Hydrodynamic interaction between approaching droplets is accounted in K_g by the collision efficiency E, whose values at the 750 mbar altitude we take from Pinsky et al (2001). Pinsky et al (2001) developed an approach to calculate the collision efficiency within a wide range of Reynolds numbers (from 0 to 100) corresponding to drops up to 300 μm radii. They calculated collision efficiency at different heights 1000, 750 and 500 mbar. They showed that the collision efficiency and the collision kernel increase significantly with height. This increase of the collision kernel is by 90% caused by the increase of the collision efficiency and 10% by the increased swept volume. This is because of the high sensitivity of collision efficiency on the relative drop-drop velocity.

3.3 Droplet distribution over sizes

It is of practical use to be able to predict the time left before rain starts given the knowledge of droplet distribution at a given instant. Such distributions can be measured with high accuracy by optical and other methods. Drop size distributions measured in many different types of clouds under a variety of meteorological conditions often exhibit a characteristic shape (Pruppacher and Klett, 1997). Generally the concentration rises sharply from low value maximum, and then decreases gently toward larger sizes, causing the distribution to be positively skewed with a long tail toward the larger sizes. We approximate such a shape with half-Gaussian $n(a,0) = \theta(a-a_0)\exp(-(a-a_0)^2/2\alpha^2)$ where θ is a step function. We thus characterize the initial distribution by two parameters: the first moment $P = \int an(a,0)\,da/n$ (mean radius) and the width σ ($\sigma^2 = \int a^2 n(a,0)\,da/n - P^2$). Since we mainly consider narrow initial distributions ($\sigma \ll P$), the rain initiation time does not depend substantially on the initial shape. We have checked that using for comparison the more commonly applied Weibull distribution (see Liu and Hallett, 1997; Liu et al, 2002) $(\lambda/\sigma)[(a-a_0)/\sigma]^{\lambda-1}\exp\{[(a-a_0)/\sigma]^\lambda\}$, for $1 \le \lambda \le 4$.

3.4 Modelling purely gravitational collisions in still air

We start from purely gravitational collisions in a still air that is solve the space-homogenous version of (2.4) with no condensation term:

$$\frac{\partial n(a)}{\partial t} = -n(a)\frac{u_g(a)}{L} + \int da'\left[\frac{K_g(a',a'')n(a')n(a'')}{2(a''/a)^2} - K_g(a',a)n(a')n(a)\right]. \tag{3.2}$$

The first term in the rhs of (3.2) models the loss of droplets falling with the settling velocity u_g from the cloud of the vertical size L. Since L are generally very large (from hundreds meters to kilometers) and $u_g(a)$ grows with a (see Figure 3.1 below), fallout is relevant only for sufficiently large drops (called raindrops) with sizes of millimeter or more. The collision (Smoluchowsky) term describes the propagation of distribution towards large sizes. The asymptotic law of propagation depends on the scaling of $K_g(a,a')$. If the collision kernel is a homogeneous function of degree α [that is $K_g(\xi a, \xi a') = \xi^\alpha K_g(a,a')$] one can show that for α larger/smaller than three the propagation is accelerating/decelerating while for $\alpha = 3$ it is exponential $\ln a \propto t$ (see van Dongen and Ernst, 1988; Zakharov et al, 1991). Our numerics show, however, that the intervals of sizes a where α is approximately a constant

are too short for definite self-similarity of the propagation to form both for narrow and wide initial distributions. This is due to complexity of both functions, $u_g(a)$ and $E(a, a')$. We thus focus on the most salient feature of the propagation, namely study how the amount of liquid water left in the cloud depends on time. Specifically we study the fraction of water left, $W = \int n(a,t)a^3\,da / \int n(a,0)a^3\,da$, relative to the value at the beginning. The decrease of that amount is due to a concerted action of collisions producing large drops and fallout.

3.5 Numerics

The droplets radii space was discretized, *i.e.* the droplets size distribution $n(a,t)$ was presented as the set of concentrations $n_i(t)$ of droplets with radius a_i. The grid of radii was taken approximately exponential at sizes that are much larger than the size of initial condensation nuclei, with 256 points in unit interval of natural logarithm. The collision term in Smoluchowsky equation was treated as follows: let the radius $(a_i^3 + a_j^3)^{1/3}$ of the droplet resulted from merging of the two with radii a_i and a_j to be in between of two radii a_k and a_{k+1} from the grid. Then the collision results in decreasing of n_i and n_j by quantity dN that is determined by the collision kernel, while the concentrations n_k and n_{k+1} are increased in such a way that sum of their change is dN and the whole amount of water in droplets is conserved in coalescence:

$$\begin{aligned}
&\delta n_i = \delta n_j = -dN = -\delta n_k - \delta n_{k+1}\,,\\
&a_k^3\delta n_k + a_{k+1}^3\delta n_{k+1} = (a_i^3 + a_j^3)dN\,,\\
&\delta n_{k+1} = dN(a_i^3 + a_j^3 - a_k^3)/(a_{k+1}^3 - a_k^3)\,,\\
&\delta n_k = dN(a_{k+1}^3 - a_i^3 + a_j^3)/(a_{k+1}^3 - a_k^3)\ .
\end{aligned} \tag{3.3}$$

The total amount of water in droplets and that left the cloud was a conserved quantity, up to 10^{-6} accuracy, during the whole simulation. In sections that deal with condensation as well, the conserved quantity is the sum of total mass of vapor, water in droplets and water that left the cloud. Note that our scheme automatically keeps the numbers positive: if dN is greater than either n_i or n_j, then we choose $dN = \min\{n_i, n_j\}$, so that n_i and n_j are also not negative after every elementary collision process. Let us stress that our scheme [1] conserves total mass of water and keeps accurate count of the number of droplets (comparing to the non-conservative scheme of Berry and Reinhardt (1974) and the scheme of Bott (1998) which was conservative only in mass and needed special choice of the time

1 Program code can be seen at http://tesla.rcub.bg.ac.yu/~vucma/mit42.c

step to keep positivity). The minimal time step needed for our calculations was estimated from characteristic timescales of our problem to be 0.1 s. We have checked that the decrease of the time step below $dt = 0.05$ s does not change the results, the figures below all correspond to that dt.

3.6 Results

We used the following values of the parameters $\nu = 0.15\,\mathrm{cm}^2 \cdot \mathrm{s}^{-1}, \rho = 1\,\mathrm{g} \cdot \mathrm{cm}^{-3}, \rho_0 = 1.2 \cdot 10^{-3}\mathrm{g} \cdot \mathrm{cm}^{-3}, g = 980\,\mathrm{cm} \cdot \mathrm{s}^{-2}$. The graphs $W(t)$ are shown at Figures 3.3 and 3.4 (for $L = 2$ km) and they are qualitatively the same both for narrow and wide initial distributions. At the initial stage, W decreases slowly due to the loss of drizzle. After large raindrops appear, loss accelerates. At every curve, the star marks the moment when respective $|d^2W/dt^2|$ are maximal (see Figure 3.4). After that moment, the cloud looses water fast so it is natural to take t_* as the beginning of rain. Figure 3.2 shows how the mass distribution over sizes, $m(a) \propto a^3 n(a)$ evolves with time (for $P = 16.7$ μm, $\sigma = 1$ μm, $L = 2$ km). One can see the appearance of secondary peaks and distribution propagating to large a. The moment t_* seems to correspond to the highest value of the envelope of the curves $m(a, t)$ of the coalescence-produced drops. One can see from Figure 3.2 that the peak at mass distribution is around 200 microns and most of the droplets are below 500 microns at $t = t_*$. The same character of the evolution $W(t)$ can be seen in the next section for the *ab initio* simulations of (2.4, 2.1).

The rain initiation time t_* defined in that way is presented in Figures 3.6 and 3.7 against the width and the mean radius of the initial distribution. Note the dramatic increase in t_* with decreasing σ for $P = 13$ μm. The mean droplet radius $P = 14$ μm is sometimes empirically introduced as the minimal size required for the onset of precipitation (Rosenfeld and Gutman, 1994). Figures 3.6 and 3.7 support that observation, they indeed show that t_* grows fast when P decreases below that size but only for very narrow initial distributions and of course there is no clear-cut threshold as $t_*(P)$ is a smooth (though steep) function. The timescales (from tens of minutes to hours) are in agreement with the data obtained before (see Pruppacher and Klett, 1997, Chapter 15; and Seinfeld, J. and S. Pandis, 1998, Chapter 15 and the references therein). Figure 3.7 also shows that for 15 μm $\lesssim P$, the function $t_*(P)$ can be well-approximated by a power law $t_* \propto P^{-\gamma}$ with $\gamma \approx 3$. The rain initiation time depends on the cloud vertical size almost logarithmically as shown in Figure 3.8, we do not have an explanation for this functional form. Let us stress that the dependence on cloud vertical size is given assuming all other parameters are fixed.

Here we treated the position and the width of the distribution as given at the beginning of the collision stage. However the distribution is itself a product of condensation stage so we now turn to the consideration of the condensation-collision mean field model.

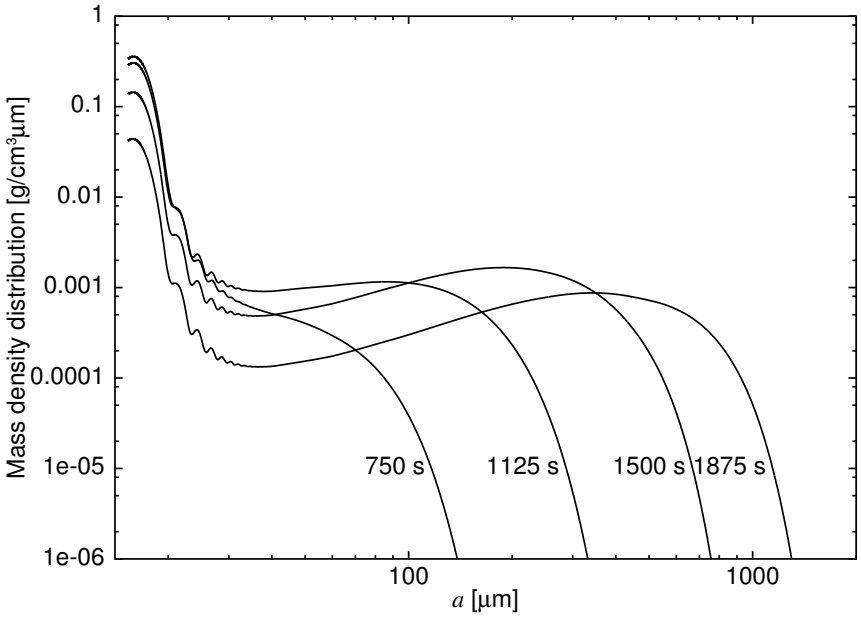

Figure 3.2: *Mass density of water shown at different moments in time, and as a function of droplet radii a. Rain initiation time is $t_* \simeq 1500$ s. Notice how with the evolution of time the largest amount of droplets moves from small radii to larger ones.*

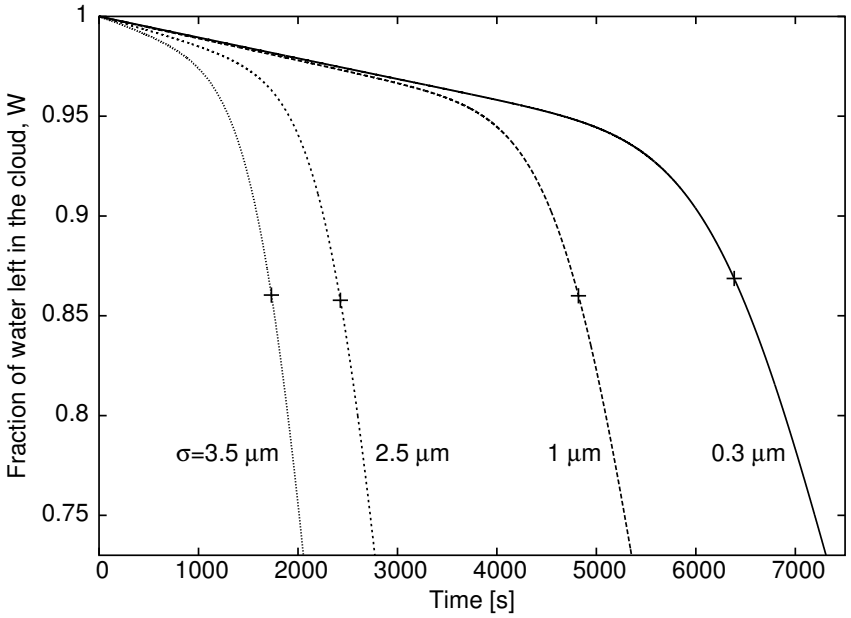

Figure 3.3: *Fraction of water left in the cloud as a function of time. The mean droplet radius of the initial distribution $n(a)$ is $P = 13$ μm. Different curves correspond to different widths σ of the initial distribution $n(a)$. Fallout of water from the cloud begins with a drizzle, which is later replaced by a faster fallout. The moments when this crossover happens are denoted with crosses and represent rain initiation times.*

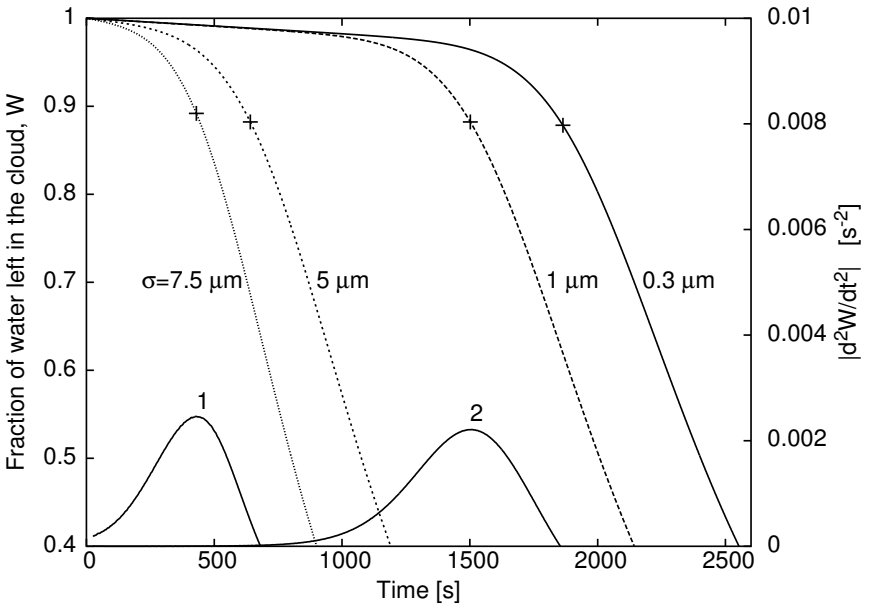

Figure 3.4: *Fraction of water left in the cloud as a function of time for the mean droplet radius of the initial distribution $n(a)$: $P = 16.7$ μm. Different curves correspond to different widths σ of the initial distribution $n(a)$. Lines 1 and 2 represent the absolute value of the second derivative of fraction of the water left in the cloud for $\sigma = 7.5$ μm and 1.0 μm respectively. Fallout of water from the cloud starts with a drizzle, which later is replaced by a faster fallout. The moments when this crossover happens are denoted with crosses, and represent rain initiation times.*

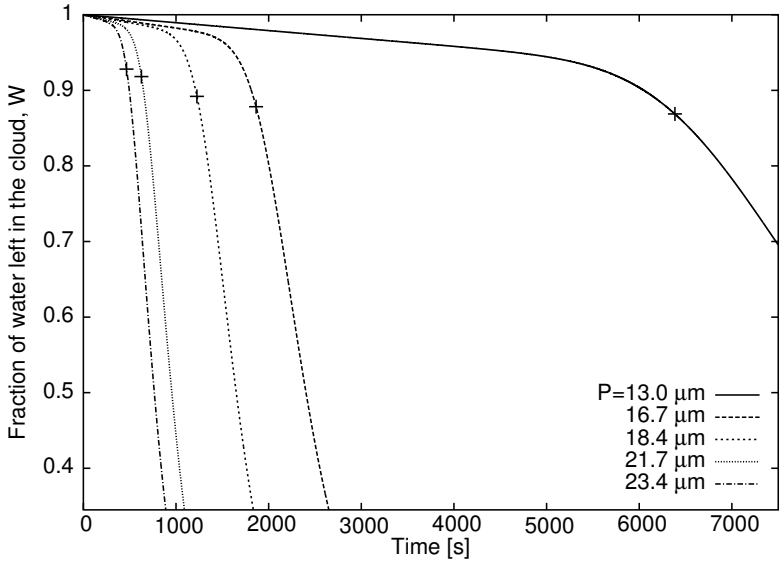

Figure 3.5: *Fraction of water left in the cloud as a function of time for the width of the initial distribution $n(a)$: $\sigma = 0.3$ μm. Different curves correspond to different mean radii P of this distribution. Initial drizzle is later replaced by a faster fallout of water from the cloud. The moments when this change happens are denoted with crosses and represent rain initiation times.*

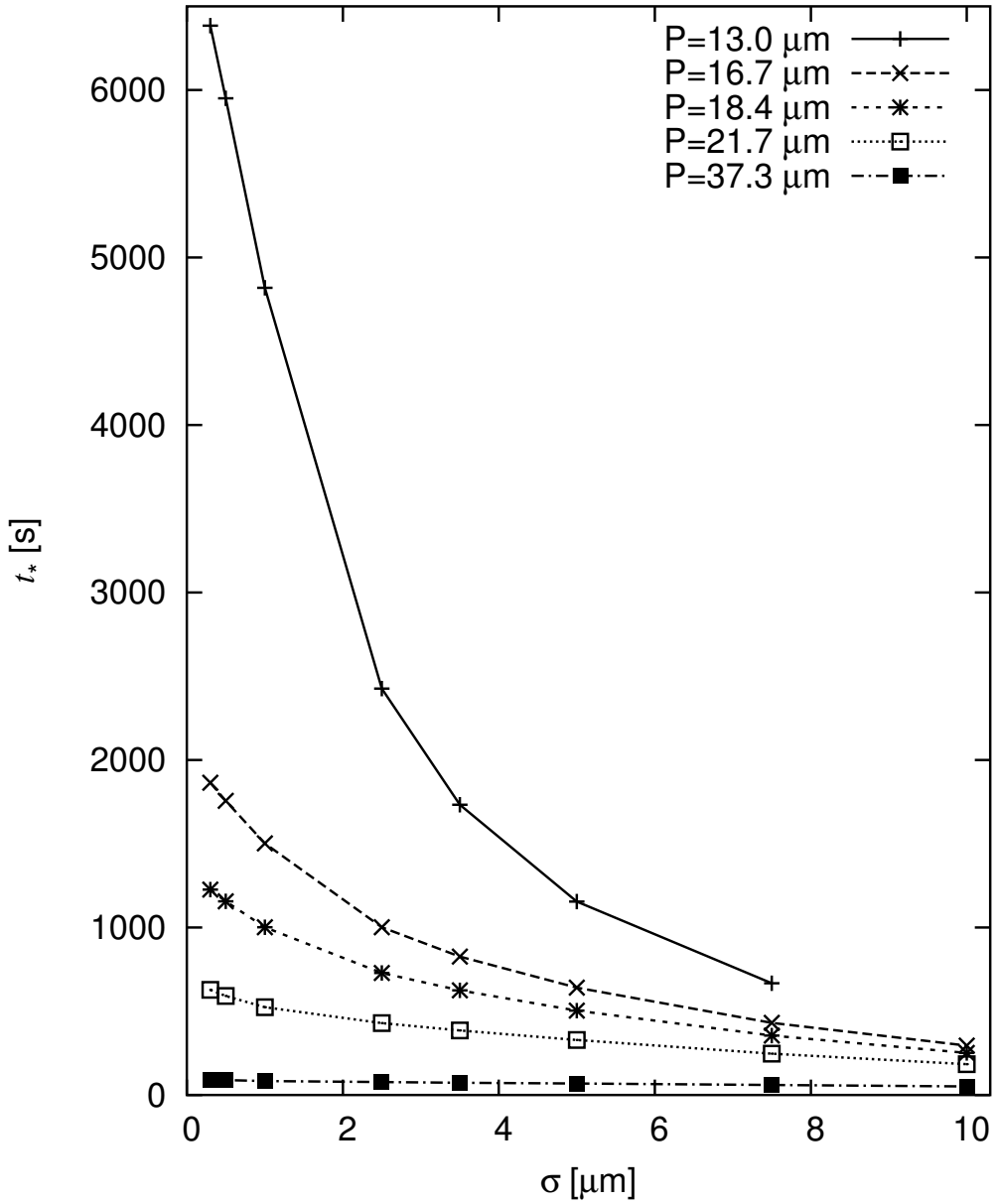

Figure 3.6: *Rain initiation time as function of the width σ of the initial distribution $n(a)$, for different mean radii P of this distribution. Notice a dramatic increase in t_* with decreasing σ for $P = 13$ μm. The mean droplet radius $P = 14$ μm is empirically introduced as the minimal size required for the onset of precipitation (Rosenfeld and Gutman, 1994).*

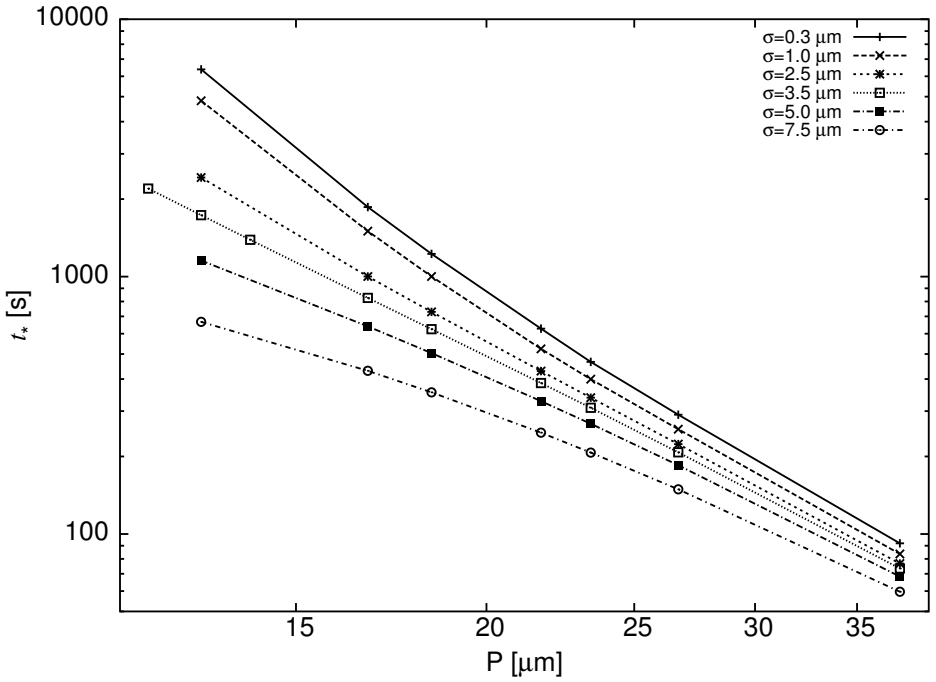

Figure 3.7: *Rain initiation time as function of the mean radius P of the initial distribution $n(a)$ for different widths σ this distribution. For 15 μm $\lesssim P$, the function $t_*(P)$ can be well-approximated by a power law $t_* \propto P^{-\gamma}$ with $\gamma \approx 3$.*

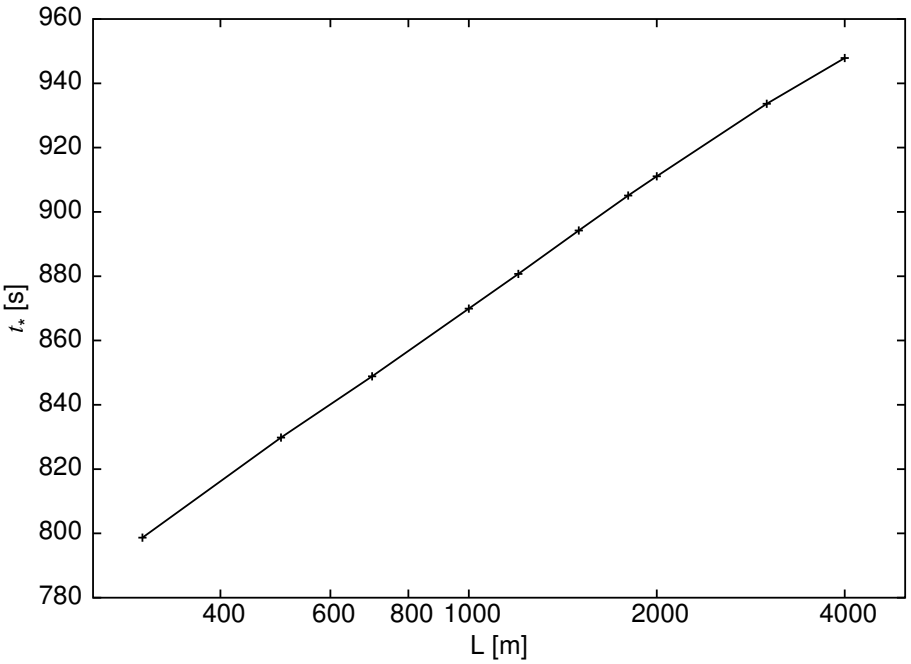

Figure 3.8: *Rain initiation time as function of the cloud vertical size L for the mean droplet radius $P = 18.8$ μm and the width $\sigma = 1$ μm) of the initial distribution $n(a)$.*

4. Condensation and collisions

We consider now the growth of droplets by condensation and collisions:

$$\frac{\partial n(a)}{\partial t} = -\frac{\kappa s M}{\rho_0}\frac{\partial}{\partial a}\frac{n(a)}{a} - n(a)\frac{u_g(a)}{L} \tag{4.1}$$
$$+ \int da' \left[\frac{K(a',a'')n(a')n(a'')}{2(a''/a)^2} - K(a',a)n(a')n(a)\right] ,$$

$$\frac{\partial M}{\partial t} = -4\pi s M \kappa \int a n(a) da \ . \tag{4.2}$$

The system (4.1, 4.2) is our mean-field model where the only memory of spatial inhomogeneities is the fallout term. Without this term, it has a form of balance relations preserving the total water content (vapor plus droplets) $W_T(t) = M(t) + 4\pi\rho_0 \int n(a,t)a^3\, da/3$. As we show here, this model gives the rain initiation times with reasonable quantitative values and proper qualitative behavior upon the change of parameters. Let us discuss first how t_* depends on the CCN number $n_0 = \int n(a,0)\, da$. Here, the most important feature is the existence of the minimum in the function $t_*(n_0)$. That can be explained by the competition between condensation, collisions and vapor depletion. Since condensation slows down and coalescence accelerates as the size of droplets grow then there exists a crossover size a_c. With a certain degree of simplification, one can say that the growth until a_c is due to condensation and after that due to collisions.

Since collisional growth accelerates with the size, an order-of-magnitude estimate for the rain initiation time is the time of condensational grows until a_c. When the CCN number is low enough it does not influence condensation yet the collisions are more frequent for higher number of droplets. That means that increasing n_0 from low values we decrease the crossover size a_c (collisions take over earlier) and thus decrease the time needed for droplet growth. Such a decrease of t_* with n_0 must go until we consider the CCN number which is large enough for vapor depletion to play the role. Vapor depletion starts to affect condensation when the amount of water in droplets is getting comparable to that in vapor, which corresponds to the droplet size $a_d \simeq (M/n_0\rho_0)^{1/3}$. When droplets grow comparable to a_d vapor depletion slows and then stops condensation. The question now is which size,

a_c or a_d, decays faster with n_0. Let us give a rough estimate for a_c. Collisions change the concentration $n(a)$ on a timescale of order $1/\int K(a,a_1)n(a_1)da_1$. Assuming that during the growth until a_c the total number of droplets did not change much (since condensation was the leading mechanism) and that all droplets have comparable sizes, we get a_c determined by the implicit relation $K(a_c)n_0 \simeq \kappa sM/\rho_0 a_c^2$. Note that for all mechanisms of collision (Brownian, gravitational and turbulent) the collision kernel $K(a)$ grows faster than a^2 so that a_c decreases with n_0 slower than $n_0^{-1/3}$. That means that for sufficiently small n_0, $a_d > a_c$ and vapor depletion is indeed irrelevant. However, for sufficiently high n_0, a_c is getting comparable to a_d and the decrease of t_* with n_0 stops. If one takes the initial concentration even larger so that $a_c > a_d$ then vapor depletion stops condensation earlier than sizes reach a_c; collisions are slower for droplets of the smaller sizes so that the overall time of droplet growth is getting larger. The concentration n_c that corresponds to the minimal time can be found from the (implicit) relation $a_d \simeq a_c$:

$$(M/n_c\rho_0)^{-1/3} K\Big[(M/n_c\rho_0)^{1/3})\Big] \simeq \kappa s\,. \tag{4.3}$$

That tells that $n_c \propto M$ and if the kernel is homogeneous, $K \propto a^\alpha$, then $n_c \propto s^{3/(1-\alpha)}$. One can argue that for small concentrations (generally for maritime clouds), $n_0 < n_c$, times of condensation and collision stages are comparable. Therefore, t_* is a function of the product Ms. For a homogeneous kernel, $t_* \propto n^{-2/(2+\alpha)}(Ms)^{-\alpha/(2+\alpha)}$. For large concentrations (generally for continental clouds), $n_0 > n_c$, the rain initiation time is mainly determined by collisions so it is getting independent of the supersaturation and $t_* \propto n_0^{(\alpha-3)/3} M^{-\alpha/3}$.

4.1 Numerics

Let us illustrate now the non-monotonic dependence of the rain initiation time of the CCN number by numerically solving (4.1, 4.2). Remark that in the effective kinetic model of McGraw and Liu (2003, 2004) the barrier-crossing rate was observed to increase with CCN and then decrease after some value. We substitute $K = K_g$ and start from CCN (*i.e.* initial droplets) uniformly distributed between 1 and 2 microns. We take $\kappa = \kappa_T = 0.25\,\mathrm{cm}^2\cdot\mathrm{s}^{-1}$, $T = 300\,\mathrm{K}$, $\mathcal{L} = 4\cdot 10^4\,\mathrm{J/mol}$ and $R = 8.3\,\mathrm{J}\cdot\,\mathrm{mol}^{-1}\cdot\mathrm{K}^{-1}$. We obtain the rain initiation time (defined by the maximum of d^2W_T/dt^2) as a function of the CCN concentration n_0 for different values of the supersaturation s and the vapor content M.

The grid of radii was approximately exponential at sizes that are much larger than the size of initial condensation nuclei (with 200 points in unit interval of natural logarithm). The condensation of vapor was taken into account by working on evolving grid of radii $a_i(t)$

keeping conserved the total mass of water in droplets and vapor. Collisions were modelled according to (3.3) described above. Note that the numerical scheme we employ here has an additional advantage (comparing to those described in Pruppacher and Klett, 1997; Berry and Reinhardt, 1974; Bott, 1998) of accounting simultaneously for condensation and collisions while respecting conservation laws. We used the time step $dt = 0.01$ s during the condensation phase, on a later stage (dominated by coalescence) $dt = 0.1$ s was enough. The same grid is used for condensation and coalescence.

4.2 Results

Those results are presented in Figure 4.1 for $L = 1$ km. The solitary point at the lower part corresponds to $M = 6$ g$\cdot$ m^{-3}, $s = 1/60$. The three solid lines correspond to $M = 3$ g$\cdot$ m^{-3} and respectively to $s = 0.0173$, 0.0086, 0.0043, from bottom to top. The three dashed lines correspond to $M = 1.5$ g$\cdot$ m^{-3} and respectively to $s = 0.0196$, 0.0076, 0.0038, from bottom to top.

We see that indeed the graphs $t_*(n_0)$ all have minima. The position of the minimum is proportional to M as expected and approximately proportional to $s^{-1/2}$ which would correspond to $\alpha \simeq 7$ in this interval of sizes. We see that the left parts of different curves with the same value of the product sk approach each other as n_0 decreases. Indeed, middle dashed line and upper solid line correspond to $k = 4 \cdot 10^{-9}\,\mathrm{cm}^2 \cdot s^{-1}$ while lower dashed line and middle solid line have $k = 2 \cdot 10^{-9}\,\mathrm{cm}^2 \cdot s^{-1}$. To the right of the minima, the curves with different s but the same M approach each other as n_0 increases. That supports the previous conclusions on the respective roles of condensation and collisions in determining the rain initiation time. Note that the ascending parts of the curves (growth of t_* with n_0) together with Figure 3.7 correspond to the so-called *second aerosol indirect effect*[1] (Squires, 1958). Being interested in the qualitative (non-monotonic) dependence $t_*(n)$ we disregarded here the turbulence contribution into the collision rate (see *e.g.* Saffman and Turner, 1956; Maxey, 1987; Squires and Eaton, 1991; Sundaram and Collins, 1997; Shaw et al, 1998; Reade and Collins, 2000; Grits et al, 2000; Vaillancourt and Yau, 2000; Kostinski and Shaw, 2001; Falkovich et al, 2002; Falkovich and Pumir, 2004; Collins and Keswani, 2004; Wang et al 2005; Franklin et al, 2005 and the references therein). For the parameters considered here, turbulence with the rms velocity gradient $\lambda \leq 15\,s^{-1}$ can only slightly diminish t_* and cannot change the qualitative form of the dependence $t_*(n)$. We

1 *Second aerosol indirect effect* - the effect that smaller cloud droplets can decrease precipitation efficiency.

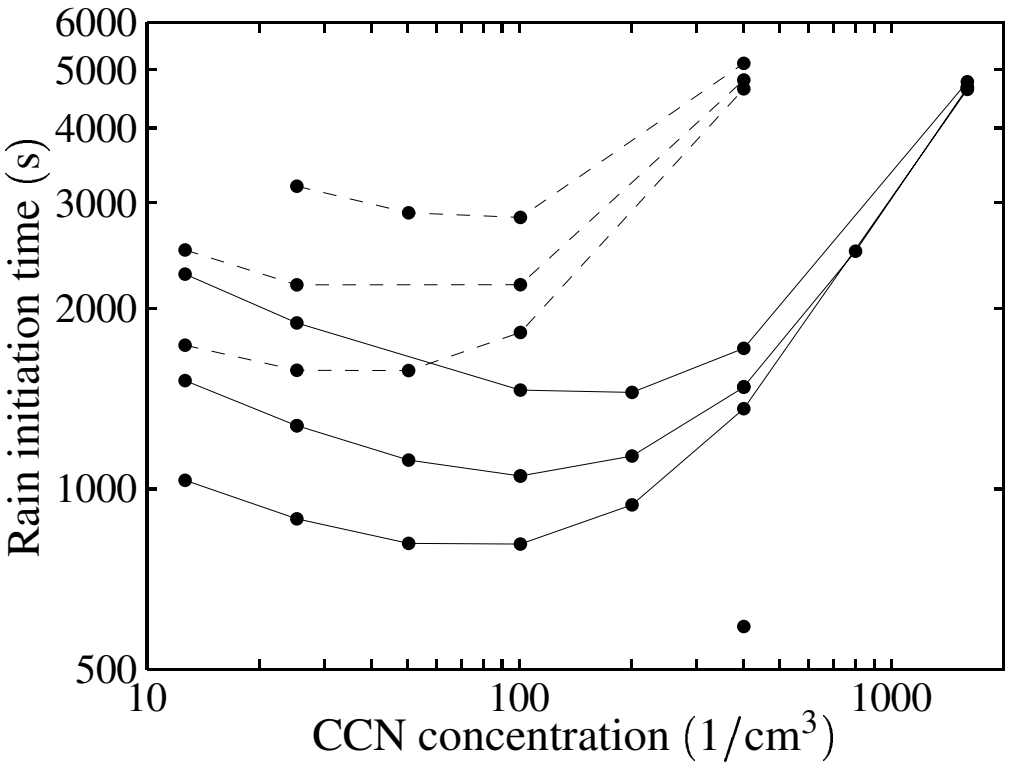

Figure 4.1: *Rain initiation time t_* as function of CCN concentration n_0 for different values of supersaturation s and water vapor density M. Notice that all $t_*(n_0)$ functions have a minimum. The characteristic cloud size is $L = 1$ km. The solitary point at the lower part corresponds to $M = 6$ g·m^{-3}, $s = 1/60$. The three solid lines correspond to $M = 3$ g· m^{-3} and respectively to $s = 0.0173, 0.0086, 0.0043$, from bottom to top. The three dashed lines correspond to $M = 1.5$ g· m^{-3} and respectively to $s = 0.0196, 0.0076, 0.0038$, from bottom to top.*

also disregard regular vertical inhomogeneity of supersaturation due to temperature profile which does not broaden $n(a)$ much even with the account of turbulence-induced random fluctuations (Korolev, 1995; Turitsyn, 2003). Spatial inhomogeneities in vapor density M due to mixing of humid and dry air remains a controversial subject (see. e.g Pruppacher and Klett, 1997; Baker et al, 1980) and probably can be neglected in cloud cores. We address the turbulent mixing of vapor in Chapter 5 considering partially seeded clouds.

5. Delaying rain by hygroscopic over-seeding

That the rain time is a non-monotonic function of the concentration of droplets may provide a partial explanation for the conflicting observations of the effect of hygroscopic seeding. By seeding clouds with hygroscopic aerosol particles one can vary the number of cloud condensation nuclei and thus the number of small droplets at the beginning of the cloud formation.

5.1 Seeding suppresses and accelerates precipitation

It was observed that seeding clouds with hygroscopic aerosol particles in some cases suppresses precipitation (see *e.g.* Rosenfeld et al, 2001), while in other cases enhances and accelerates it (Cotton and Pielke, 1995; Mather, 1991), see also Bruintjes (1999) for a recent review.

Rosenfeld et al (2001) have observed that the effect of dust on cloud properties is to inhibit precipitation, contrary to theoretical models, which predicted that rainfall would be enhanced. Using satellite and aircraft observations they showed that clouds forming within desert dust contain small droplets and produce little precipitation by drop coalescence. They measured the size distribution and chemically analyzed individual Saharan dust particles collected in the dust storm. The detrimental impact of dust on rainfall was smaller than that caused by smoke from biomass burning or anthropogenic air pollution, but the large abundance of desert dust in the atmosphere rendered it important. The authors concluded that the reduction of precipitation from clouds affected by desert dust can cause drier soil, which in turn raises more dust, thus providing a possible feedback loop to further decrease of precipitation. Furthermore, anthropogenic changes of land use exposing the topsoil can initiate such a desertification feedback process.

Mather (1991) "spotted" a storm whose microphysical characteristic were recognized

as so unusual against an extensive microphysical database, that some explanation was needed for the apparent errant behavior of this storm. The probable cause was attributed to emissions from a Kraft paper mill 10 km south of the storm's position. The mill had undergone an expansion program that had quadrupled its output of paper products. Using the radar characteristics of this unusual storm as a guide, a search of one season of radar data revealed the existence of five other similar storms, all within about 30 km of the paper mill. These records indicated that the storms apparently modified by the paper mill tended to last longer, grow taller, and rain harder than any other storms recorded that day. The most singular feature of the modified storms was the appearance of large (> 4 mm) drops at the most common sampling level ($-10°$C), indicating an accelerated or enhanced coalescence precipitation formation process.

5.2 Postponing rain

It is often desirable to postpone rain, for instance to bring precipitation inland from the sea. The fact that t_* grows with n when $n_0 > n_c$ suggests the idea of over-seeding to delay rain. This is considered to be unpractical: "It would be necessary to treat all portions of a target cloud because, once precipitation appeared anywhere in it, the raindrops ... would be circulated throughout the cloud ... by turbulence" (Dennis, 1980). We think that this conclusion ignores another, positive aspect of cloud turbulence, namely the mixing and homogenization of partially seeded cloud during the condensation stage. We describe briefly how it works for two cases.

Consider first seeding a part of the cloud comparable to its size L_c. Note that we do not consider here adding ultra-giant nuclei, we assume seeded CCN to be comparable in size to those naturally present. Two fluid parcels at first increase their distance exponentially (since the air velocity on such lengths can be considered spatially smooth), therefore the rms difference of vapor concentrations decreases exponentially (it behaves as one over the square root of the volume). Later, at times $t^3 > t_0^3 = L_c^2/\epsilon$ (ϵ is the energy dissipation rate in turbulence), the squared distance between two fluid parcels grows according to the Richardson law as ϵt^3, so the rms difference of vapor concentrations between seeded and unseeded parts decreases as $t^{-9/4}$. To see how different rates of condensation interplay with turbulent mixing we generalize the mean-field system (4.1, 4.2) describing seeded and unseeded parts by their respective n_1, n_2 and $x_1 = s_1 M_1$, $x_2 = s_2 M_2$ and link them by adding the term that models the decay of the difference: $dx_i/dt = \ldots - (x_i - x_j)t(t + t_0)^{-2}(9/4)$. Note that at $t \ll t_0$ we have $dx_i/dt \propto -(x_i - x_j)t$ that gives exponential

decrease of the rms difference of vapor concentrations, while at $t \gg t_0$ the rms difference of vapor concentrations changes as $dx_i/dt \propto -(x_i - x_j)/t$, which corresponds to the estimate obtained from Richardson law.

As a crude model, we assume two parts to evolve separately until $t = 2t_0$, then we treat the cloud as well-mixed and allow for the collisions between droplets from different parts. That actually underestimates the effect of seeding and can be considered as giving the lower bound for the time before rain. The results of simulations are shown in Figure 5.1 for $t_0 = 180$ s, $L = 1$ km and $\lambda = 15$ s^{-1}. It is seen from Figure 5.1A that the total water content W_T changes similarly to what was shown in Figures 3.3 and 3.4 and the rain initiation time is again determined by the maximum of d^2W_T/dt^2. The respective times are shown against $n_0 = (n_1 + n_2)/2$ by boxes in Figure 5.1B. The time increase is less than for homogeneously seeded one, but it is still substantial. The fraction of the cloud still unmixed after the time t decreases by the Poisson law $\exp(-t/t_0)$. Taking $n_1 = 100$ cm^{-3} one sees that for a time delay of 10 min one needs to seed by $n_2 \simeq 3000$ cm^{-3}.

Second, consider seeding by N particles a small part of the cloud which (unseeded) had some n_0 and would rain after t_*. After time t_* the seeds spread into the area of size $(\epsilon t_*^3)^{1/2}$ with the concentration inside the mixed region decaying as $n(t_*) = N(\epsilon t_*^3)^{-3/2}$ (for stratiform clouds one gets $N(\epsilon t^3)^{-1}$). To have an effect of seeding, one needs $n(t_*) > n_0$ which requires $N > 10^{15}$ for $n_0 = 50$ cm^{-3}, $t_* = 10$ min and $\epsilon = 10$ cm$^2 \cdot$ s^{-3}. With sub-micron particles weighing 10^{-11} g that would mean hundreds of kilograms, which is still practical.

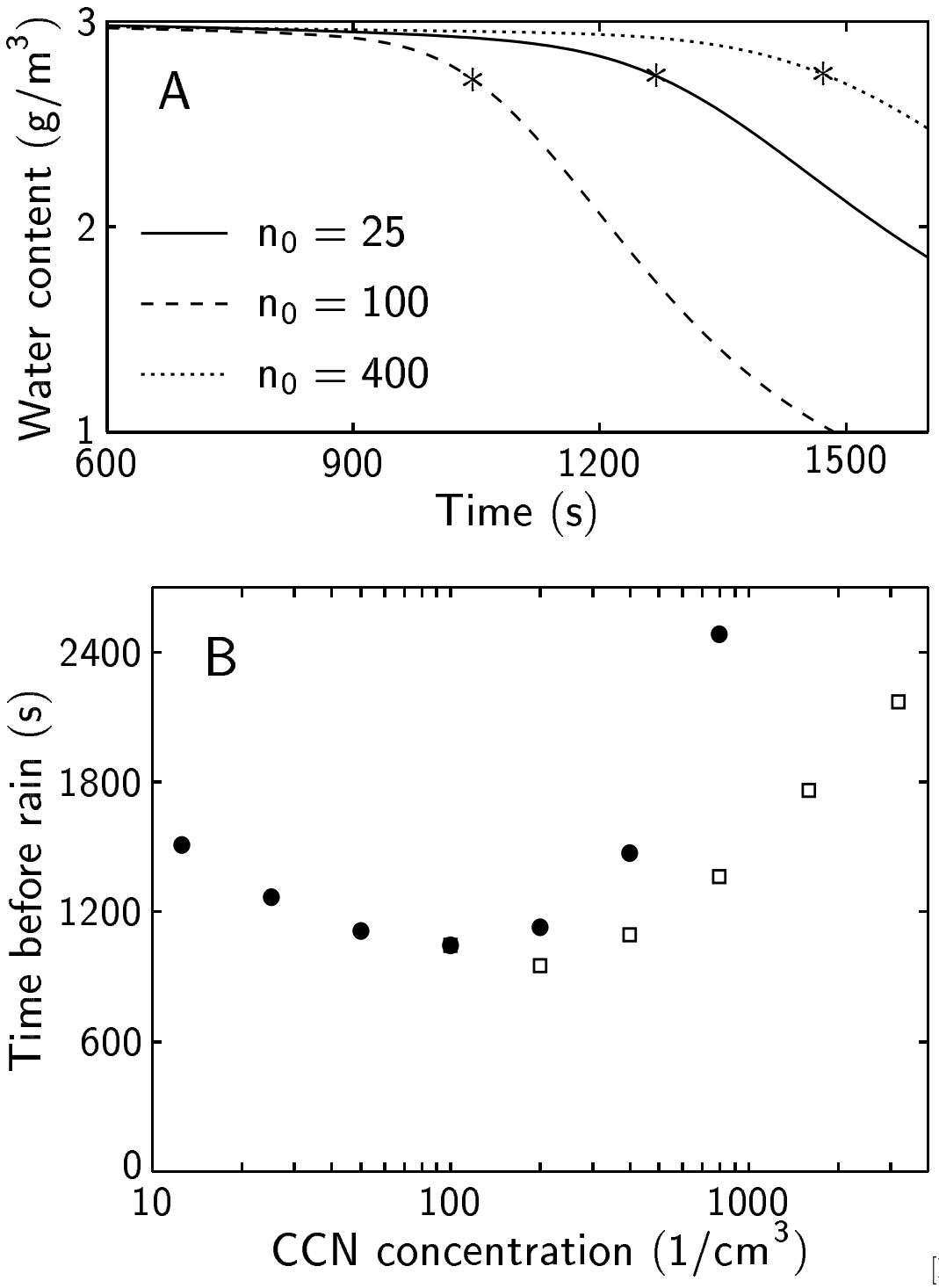

[h]

Figure 5.1: *Fraction of water left in the cloud as a function of time is shown in (A). The asterisk signs mark rain initiation times t_*, times when the slow drizzle fallout of water from the cloud is replaced by a more rapid one. Rain initiation time t_* as a function of CCN concentration n_0 is shown in (B). The lower part (boxes) corresponds to a half-seeded cloud (the half-sum of concentrations is used as abscissa) while the upper part (filled circles) corresponds to an unseeded one. The time increase for a half-seeded cloud is less than for homogeneously seeded one, but it is still substantial. Notice that seeding a bit can accelerate rain, but taking e.g. $n_1 = 100$ cm^{-3} and seeding with $n_2 \simeq 3000$ cm^{-3} would cause a postponement of rain of about 10 min.*

6. Summary

We believe that our main result is a simple mean-field model (4.1, 4.2) which demonstrates non-monotonic dependence of the rain initiation time on CCN concentration. As the CCN concentration increases, the rain initiation time first decreases and then grows as shown in Figures 4.1, 5.1. The modification of this model for an inhomogeneous case, described in Section 5, shows that one can increase the rain initiation time even for a cloud partially seeded by hygroscopic aerosols. We estimate that such seeding is practical. Possible application would be to postpone the rain initiation time of maritime clouds, so that they precipitate over mainland of Israel and not over the Mediterranean sea, as usually happens.

Appendix A Table of definitions of variables

Quantity	Units	Description
a	cm	Droplet radius
c	$\mathrm{J{\cdot}K^{-1}}$	Heat capacity of dry air at constant pressure
$\mathbf{f}$	N	Boundary driven forces
$\mathbf{g}$	$\mathrm{cm{\cdot}s^{-2}}$	Acceleration of gravity
K	$\mathrm{cm^3{\cdot}s^{-1}}$	Collision kernel
L	cm	Cloud vertical size
$\mathcal{L}$	$\mathrm{J{\cdot}mol^{-1}}$	Latent heat of condensation
L_e	$\mathrm{J{\cdot}g^{-1}}$	Latent heat of evaporation of water per unit mass
M	$\mathrm{g{\cdot}cm^{-3}}$	Water vapor density
$\mathcal{M}_{\mathcal{W}}$	$\mathrm{g{\cdot}mol^{-1}}$	Molecular weight of water
$n(a)$	$\mathrm{cm^{-4}}$	Distribution of droplet sizes in a unit volume
p	Pa	Athmospheric pressure
P	cm	Mean radius of the initial distribution $n(a)$
$\mathbf{r}$	cm	Spatial coordinate
R	$\mathrm{J{\cdot}mol^{-1}{\cdot}K^{-1}}$	Universal gas constant
R_{e_a}	#	Reynold's number
s	#	Supersaturation
t	s	Time
t_*	s	Rain initiation time
T	K	Temperature
$\mathbf{u}$	$\mathrm{cm{\cdot}\ s^{-1}}$	Air velocity
$\mathbf{u}_g$	$\mathrm{cm{\cdot}\ s^{-1}}$	Terminal fall velocity
$\mathbf{v}$	$\mathrm{cm{\cdot}\ s^{-1}}$	Cloud particle velocity
W	#	Relative amount of water in the cloud
β	$\mathrm{K^{-1}}$	Coefficient linking density changes with temperature changes
κ	$\mathrm{cm^2{\cdot}s^{-1}}$	Water vapor diffusivity
κ_T	$\mathrm{cm^2{\cdot}s^{-1}}$	Thermal conductivity
ν	$\mathrm{cm^2{\cdot}s^{-1}}$	Kinematic air viscosity
ρ	$\mathrm{g{\cdot}cm^{-3}}$	Air density
ρ_0	$\mathrm{g{\cdot}cm^{-3}}$	Liquid water density
σ	cm	Width of the initial distribution $n(a)$

Table A.1: *Definitions of variables*

References

[1] AMS, *Glossary of Meteorology*, the electronic version of the second edition: http://amsglossary.allenpress.com/glossary, AMS, 2000.

[2] Baker M. B., Corbin, R. G. and J. Latham, 1980: The effects of turbulent mixing in clouds, *Quart. J. Roy. Meteor. Soc.* **106**, 581–598.

[3] Berry, E. X. and R. L. Reinhardt, 1974: An analysis of cloud drop growth by collection, *J. Atm. Sci.* **31**, 1814–2127.

[4] Bott, A., 1998: A flux method for the numerical solution of the stochastic collection equation *J. Atm. Sci.* **55**, 2284–2293.

[5] Beard, K. V., Durkee, R. I. and H. T. Ochs, 2002: Coalescence efficiency measurements for minimally charged cloud drops, *J. Atm. Sci.* **59**, 233–243.

[6] Bruintjes, R. T., 1999: A review of cloud seeding experiments to enhance precipitation and some new prospects, *Bull. Amer. Met. Soc.* **80**, 805–820.

[7] Collins, L. R. and A. Keswani, 2004: Reynolds number scaling of particle clustering in turbulent aerosols, *New Journal of Physics* **6**, Art. 119.

[8] Cotton, W. R., and R. A. Pielke, 1995: *Human impacts on weather and climate*, (Cambridge Univ. Press, New York).

[9] Dennis, A. S., 1980: *Weather modification by cloud seeding* (Acad. Press, New York).

[10] Falkovich, G., Fouxon, A., and M. G. Stepanov, 2002: Acceleration of rain initiation by cloud turbulence, *Nature* **419**, 151–154.

[11] Falkovich, G. and A. Pumir, 2004: Intermittent distribution of heavy particles in a turbulent flow. *Phys. Fluids* **16**, L47–50.

[12] Franklin, C., Vaillancourt, P., Yau, M. K., and P. Bartello, 2005: Collision Rates of Cloud Droplets in Turbulent Flow, *J. Atm. Sci.* **62**, 2451–2466.

[13] Grits, B., Pinsky, M. and A. Khain, 2000: Formation of small-scale droplet concentration inhomogeneity in a turbulent flow as seen from experiments with an isotropic turbulence model *Proc. 13th Int. Conf. on Clouds and Precipitation.*

[14] Gunn, R., and G. D. Kinzer, 1949: The terminal velocity of fall for water droplets in stagnant air, *J. Meteor.* **6**, 243–248.

[15] Korolev, A., 1995: The influence of supersaturation fluctuations on droplet size spectra formation, *J. Atm. Sci.* **52**, 3620–3634.

[16] Kostinski, A., and R. Shaw, 2001: Scale-dependent droplet clustering in turbulent clouds, *J. Fluid Mech.* **434**, 389–398.

[17] Liu, Y. G. and J. Hallett, 1997: The '1/3' power law between effective radius and liquid-water content, *Quart J. Roy. Met. Soc*, **123**, 1789–1795. Liu, Y. G., Daum, P. H., and J. Hallett, 2002: A generalized systems theory for the effect of varying fluctuations on cloud droplet size distributions, *J. Atmos. Sci.* **59**, 2279–2290.

[18] Mather, G. K., 1991: Coalescence enhancement in large multicell storms caused by the emissions from a Kraft paper mill, *J. Appl. Met.* **30**, 1134–1146.

[19] Maxey, M. R., 1987: The gravitational settling of aerosol particles in homogeneous turbulence and random flow field, *J. Fluid Mech.* **174**, 441–465.

[20] McGraw, R. and Y. Liu, 2003: Kinetic Potential and Barrier Crossing: A Model for Warm Cloud Drizzle Formation, *Phys. Rev. Lett.* **90**, 018501–4.

[21] McGraw, R. and Y. Liu, 2004: Analytic formulation and parametrization of the kinetic potential theory for drizzle formation, *Phys. Rev. E* **70**, 031606–19.

[22] Pinsky, M., Khain, A. and M. Shapiro, 2001: Collision efficiency of drops in a wide range of Reynolds numbers, *J. Atm. Sci.* **58**, 742–766.

[23] Pruppacher, H. R. and J. D. Klett, 1997: *Microphysics of Clouds and Precipitation* (Kluwer Acad. Publ., Dordrecht, ed. 2).

[24] Reade, W. and L. Collins, 2000: Effect of preferential concentration on turbulent collision rates, *Phys. Fluids* **12**, 2530–2540.

[25] Rosenfeld, D. and G. Gutman, 1994: Retrieving microphysical properties near the tops of potential rain clouds by multispectral analysis of AVHRR data, *Atmos. Res.* **34**, 259–283.

[26] Rosenfeld, D., Rudich, Y. and R. Lahav, 2001: Desert dust suppressing precipitation: A possible desertification feedback loop, *Proc. Nat. Ac. Sci. U.S.A.* **98**, 5975–5980.

[27] Saffman, P. and J. Turner, 1956: On the collision of drops in turbulent clouds, *J. Fluid Mech.* **1**, 16–30.

[28] Seinfeld, J. and S. Pandis, 1998: *Atmospheric Chemistry and Physics* (John Wiley and Sons, NY).

[29] Shaw, R. 2003: Particle-turbulence interaction in atmospheric clouds, *Ann. Rev. Fluid Mech.* **35**, 183–227. Shaw, R., Reade, W., Collins, L. and J. Verlinde, 1998: Preferential concentration of cloud droplets by turbulence: effect on early evolution of cumulus cloud droplet spectra. *J. Atmos. Sci.* **55**, 1965–1976.

[30] Squires, K., 1958: The microstructure and colloidal stability of warm clouds, *Tellus* **10**, 256–261.

[31] Squires, K. and J. Eaton, 1991: Measurements of particle dispersion from direct numerical simulations of isotropic turbulence, *J. Fluid Mech.* **226**, 1–35.

[32] Sundaram, S. and L. Collins, 1997: Collision statistics in an isotropic particle-laden turbulent suspension, *J. Fluid Mech.* **335**, 75–109.

[33] Turitsyn, K. S., 2003: Air parcel random walk and droplet spectra broadening in clouds, *Phys. Rev. E* **67**, 062102–3.

[34] Vaillancourt, P. A. and M. K. Yau, 2000: Review of particle-turbulence interactions and consequences for cloud physics, *Bull. Amer. Met. Soc.* **81**, 285–298.

[35] van Dongen, P. G. J. and M. H. Ernst, 1988: Scaling solutions of Smoluchowski's coagulation equation, *J. Stat. Phys.* **50**, 295–328.

[36] Wang, L-P., Ayala, O., Kasprzak, S. and W. Grabowski, 2005: Theoretical Formulation of Collision Rate and Collision Efficiency of Hydrodynamically Interacting Cloud Droplets in Turbulent Atmosphere, *J. Atmos. Sci.* **62**, 2433–2450.

[37] Zakharov, V., Lvov, V. and G. Falkovich, 1992: *Kolmogorov Spectra of Turbulence* (Springer-Verlag, Berlin).

Acknowledgments

I would like to thank Grisha Falkovich for the opportunity to work with him on this interesting and important topic. His intuition of the physical problem has been an excellent guidance. I would also like to thank Misha Stepanov for insightful discussions and help with programming and Sasha Fouxon for useful suggestions and excellent questions related to my research. They inspired me tremendously both as a person and as a physicist.

Најлепше Вам хвала, Маша!
The "most beautiful" thank You, Masha!